

ASTRONOMICAL FOURIER TRANSFORM SPECTROSCOPY REVISITED

S. T. Ridgway and J. W. Brault

Kitt Peak National Observatory,¹ Tucson, Arizona 85726

1. INTRODUCTION

The Fourier transform spectrometer (FTS) has joined the ranks of a small number of general purpose, high-performance spectroscopic instruments now available to astronomers. As with any technique, the FTS has advantages and disadvantages in comparison with other current or potential experimental methods. The principal objective of this review is to introduce the FTS and to discuss both its demonstrated capabilities and its limitations for astronomical measurements. A very brief introduction to the optical characteristics of the FTS is followed by a point-by-point consideration of the distinctive features of the FTS that make it attractive or unattractive for particular astronomical applications. To further clarify the possible uses of the technique, the final section of the review describes in some detail numerous successful applications of the FTS.

It is more than a decade since Pierre Connes (17) reviewed Fourier spectroscopy in this annual. At that time he remarked, "Thus the time for reviewing the subject seems ripe; hopefully a few years from now it may be impossible to cover entirely." This has indeed proved to be the case, and it is not feasible to include within this review all of the important developments of the past 14 years. Thus we frequently refer to other recent reviews that cover some topics in more depth.

¹ Operated by the Association of Universities for Research in Astronomy, Inc., under contract with the National Science Foundation.

2. THE INSTRUMENT

2.1 *The Optical and Mechanical Implementation*

An FTS is simply a Michelson interferometer with variable path difference between the two arms. Nevertheless, the FTS has long had the reputation of being both esoteric and phenomenally expensive. The former assessment is no doubt a consequence of the hesitation of many astronomers to think in Fourier transform space a decade or more ago. This faintness of heart is less widespread today. The cost of the technique derives from the necessity to provide physical motion with interferometric tolerances (which can still be expensive), and the need for a computer to extract a spectrum from the data (which is no longer so costly). But fundamentally, when the FTS was introduced, astronomers simply were not used to the cost of the high technology that is now taken for granted in image intensifiers, array detectors, and customized electronics. By modern standards the FTS can no longer be considered highly esoteric, exceptionally difficult to fabricate, or remarkably expensive.

In the actual fabrication of an FTS, the driving factors in cost and complexity are the design wavelength and the resolution. The former determines the required tolerances, the latter the required scale. The principal design problems are the support of the beam splitter and the mechanisms for varying the optical path difference between the two arms. Some examples of several operating FTS systems demonstrate the range of possibilities:

1. A simple and inexpensive FTS for modest resolution in the IR has been developed and operated at Steward Observatory by Thompson (88). Plane mirrors (as in the classical Michelson) are transported on a commercial mechanical slide with a screw under torque motor control.
2. A high-resolution FTS with cat's-eye retroreflectors transported on air bearings has been developed and operated at the University of Arizona Lunar and Planetary Laboratory (18); the instrument was built for airborne and ground-based use. This group has also operated a moderate-resolution FTS at many telescopes over a period of more than a decade (56).
3. Hall and Ridgway have developed a high-resolution FTS for coudé operation at the KPNO Mayall telescope. It employs cat's-eye retroreflectors translated on a wheeled carriage and flexible parallelogram, respectively (38).
4. Brault has developed a high-resolution FTS designed for any wavelength from the UV to the IR. Cat's-eye retroreflectors are translated on

oil bearings, with the whole installed in a vacuum tank. It operates in a laboratory environment at the KPNO McMath Solar Telescope (9).

Other designs have been executed for astronomical use, both on the ground and in a host of other environments, including balloon, satellite, and spacecraft operation (e.g. 4, 43).

2.2 *Characteristics of a Modern FTS*

A modern FTS has a number of instrumental characteristics that make it a powerful tool for astronomical observations. None of these characteristics is unique to the FTS method: some have been realized in other types of spectroscopy; some that have not been realized elsewhere could be. For a more extended discussion of the comparison between the FTS and alternative methods of high-resolution spectroscopy, see Brault (11).

2.2.1 THROUGHPUT A classic feature of the FTS, shared with the Fabry-Perot interferometric spectrometer, is a large throughput or étendue (the product of solid angle and aperture of the spectrometer). In practical terms, the FTS has a circular entrance aperture rather than an entrance or exit slit. In any large FTS, the field of view for even very high resolution is substantially greater than the typical seeing disk. In fact, the tolerable solid angle is in practice usually limited not by the desired resolution but by other considerations. For extended sources, the scientific objective generally compels a restricted aperture (near the seeing limit) because, whether for the Sun, planets, or nebulae, spatial resolution is useful in the observation. (One notable exception is the study of the Sun as a star, where no image at all is formed.) For point sources, the photon noise of the sky background discourages the use of a large field of view. In laboratory spectroscopy, on the other hand, where we are dealing with homogeneous extended sources, the extra throughput of a large field of view can be extremely valuable, as the FTS can often accept 10–1000 times more source flux than the grating spectrograph.

Another factor contributing to high throughput is the inherent high efficiency of the FTS technique. A carefully selected beam splitter can easily have an efficiency exceeding 90%. Overall telescope plus FTS transmission of 25% of the incident flux may be reasonably expected.

2.2.2 SIGNAL-TO-NOISE A number of characteristics tend to protect FTS spectra from degradation due to external disturbances. Rapid scanning or modulation of the FTS places the data frequencies in selected ranges of tens to thousands of hertz. Since frequencies associated with atmospheric scintillation are typically lower than this and have a power spectrum generally proportional to $1/f$, it is convenient to place the data in a

frequency range where the atmospheric disturbances (not to mention telescope and building vibrations) are negligible.

Another related factor is the simultaneity of the observation. Although the FTS is a scanning instrument, it is scanning in *Fourier space*, and hence all spectral elements are observed simultaneously. This greatly reduces the effect of guiding errors in astronomical observations, or of source variations in laboratory measurements. In some cases the simultaneity is an essential feature of the experimental objective.

Internal normalization of the data further reduces the sensitivity of a measurement to variations of any kind in source flux (e.g. guiding errors): since the two detectors always detect all the flux in the passband, a ratio of the interferogram to the current total flux level provides a complete correction for source intensity variations that are common to all wavelengths.

Another method of reducing instrument sensitivity to irregularities in the atmosphere is the use of the common dual input aperture scheme, which provides continuous internal sky subtraction within the optical system prior to detection of the signal. This technique typically reduces the sky contamination by a factor of 50, and standard aperture switching techniques readily accommodate the residual second-order sky correction, resulting in a total cancellation factor of 10^3 – 10^4 .

A very important consideration. The discrete diode detectors commonly used in an FTS have an extremely large dynamic range (typically 10^6). Furthermore, the FTS is inherently insensitive to nonlinearities in its detector, since their main effect is to produce sidebands that are typically outside the spectral passband.

All of the factors just cited, and some of those discussed below, contribute to the capability of the FTS to obtain spectra of very high signal-to-noise ratio. Of course, the FTS cannot exceed the fundamental limit due to a finite number of photons per spectral element. Some of the factors listed above help to maximize the use of the photons that enter the telescope. Other spectrometric techniques used in astronomy are inherently limited in the obtainable signal-to-noise, even in the case of arbitrarily large source flux. The fact that the FTS records data that are self-normalized, simultaneous throughout the passband, and rapidly scanned in Fourier space contributes to the very high values of signal-to-noise. As seen in the examples below, signal-to-noise ratios of hundreds, thousands, even tens of thousands to one are achieved.

2.2.3 QUALITY A spectrograph must be judged in part by the quality of the spectra it produces, measured by how closely they approximate the result achieved by an ideal instrument. Several features of the FTS tech-

nique contribute to make it the standard against which other techniques must be judged.

The instrumental line profile is explicitly determined by easily controlled characteristics of the instrument and the observation, and in general it is possible to obtain a measurement in which the form of the profile is known analytically.

Scattered light, the bane of all grating spectrographs, does not exist in an FTS. Its closest analogue is a low-resolution feature due to nonlinearity in the detector system, which produces second harmonic and intermodulation products. If the region of interest covers a wavelength range of no more than 3 : 2, then all of these unwanted sidebands may be ignored.

The FTS offers a unique capability for frequency calibration. The simultaneous measurement in Fourier space of all frequencies ensures a uniform frequency calibration throughout the passband. Frequency precision of a few parts in 10^7 is readily obtained; this corresponds directly to a velocity of $\sim 100 \text{ m s}^{-1}$. The accuracy of relative frequency determinations is usually signal-to-noise limited, and, as indicated above, the signal-to-noise can be very high; for the Sun, frequency accuracy of $1 : 10^8$ is possible.

Another feature of the FTS, and one of the most important, is the ease with which high resolution may be obtained. In fact, existing FTS instruments readily achieve resolution sufficient to completely resolve the most narrow spectral structures known in stellar, planetary, and nebular spectra. In such cases, the instrumental profile becomes irrelevant, since no distortion of the spectrum is introduced by the spectrometer.

The combination of these characteristics permits the FTS to obtain spectra of unparalleled quality. Combined with the earlier characteristics of high throughput and high signal-to-noise, these properties enable the FTS to produce the nearest thing available to definitive spectra of astronomical sources.

2.2.4 PHOTOMETRIC ACCURACY A number of characteristics of the FTS make it a suitable instrument for recording photometric information. Rapid scanning and simultaneity of coverage reduce photometric errors. The typical use of a field of view substantially greater than the seeing disk minimizes photometric errors due to guiding. The internal normalization of the interferogram improves the accuracy of relative photometry within the bandpass (though contributing nothing to the calibration of the integrated bandpass). In addition, the very wide bandwidth typically achieved in FTS spectroscopy permits relative photometry over a substantial frequency range during a single measurement. It is also significant that the resolution of an FTS measurement is continuously variable from very low to very high in a simple and natural way. This means that low-resolution measurements

of even faint photometric standards can be obtained in a fraction of the time spent on high-resolution measurements of program objects.

The large achievable bandwidth of high-resolution spectra also contributes unique capabilities. Photometric measurement of fluxes can be obtained for the narrow continuum points detected only with the highest resolution. Accurate interpolation of a continuum from distant portions of the spectrum is possible.

2.2.5 INSTRUMENTAL FLEXIBILITY The FTS possesses many features that make it very flexible and adaptable for a variety of spectroscopic measurements, including the photometric character of the data, the variable resolution, and the availability of large field of view. Polarimetry may be added to the measurement in an elegant way to provide high-resolution polarimetric information (9, 87). Furthermore, the standard FTS configuration produces a stigmatic image of the input field at the output, permitting a variety of multiple-detector arrangements.

2.2.6 MULTIPLEXING CHARACTER OF THE FTS As traditionally implemented, the FTS puts the full spectral band on a single detector in each of two output beams. Since each spectral element is encoded in the data at a distinct electrical frequency (multiplexed), the spectrum can be extracted. If the sensitivity is limited by photon noise (from noise or background), the speed of the FTS observation will be comparable to the speed of a single-detector scanning spectrometer. Therefore, in the visible the FTS may be slow compared with multidetector instruments. Use of the FTS at short wavelengths is thus motivated by other instrumental features (e.g. throughput, resolution, wavelength accuracy).

For the range 1.1–2.5 μm , spectroscopic measurements of faint sources are often limited by detector noise. In this case the FTS has a “multiplex advantage,” owing to the fact that it does record a large range of spectrum simultaneously with one detector. The gain in speed compared with a scanning spectrometer can be about 10^4 with current detectors. This speed advantage will diminish as improved IR detectors become available.

3. EXAMPLES OF FTS LABORATORY AND ASTRONOMICAL OBSERVATIONS

In this section we provide a range of examples that will allow the reader to extrapolate to different observational or laboratory projects. First, the proportionalities that govern the determination of signal-to-noise in the FTS method are indicated, followed by a presentation of some illustrated examples for a diversity of measurements. Details of instrumental and observational parameters are provided in the figure captions. In organizing

the observational results, the emphasis is on the astronomical objective in preference to instrumental considerations.

For the purposes of scaling the performance of the FTS, the following expression will be useful:

$$\frac{S}{N} \approx \delta_{\sigma} t^{1/2} \begin{cases} F_{\sigma} \Delta_{\sigma}^{-1/2}, & 1. \\ F_{\sigma}, & 2. \\ F_{\sigma}^{1/2} \Delta_{\sigma}^{-1/2}, & 3. \end{cases}$$

where δ_{σ} is the resolution element width, t is the integration time, F_{σ} is the flux per spectral element, and Δ_{σ} is the full spectral bandpass on a single detector. The three equations refer to observations where the dominant noise source is (1) thermal background, (2) detector noise, and (3) source photon noise. To assist in determining which is the case, Figure 1 shows the boundaries between these three situations for a variety of possible parameters.

3.1 Solar and Stellar Studies

Nowhere is the close relation between solar, stellar, and laboratory science more evident than in the area of high-resolution spectroscopy. It is now possible to obtain spectral resolution and signal-to-noise on bright stars that were obtainable only for the Sun just a few years ago. And for both the Sun and stars, spectra of laboratory quality are often achieved.

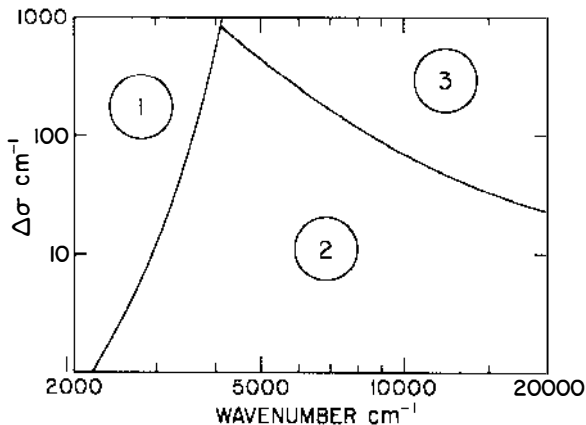


Figure 1 Signal-to-noise should be scaled according to Equation 1, 2, or 3 depending on the region of this figure in which the observation lies. The boundary between regions 2 and 3 is for magnitude $M = 7$. For other magnitudes, shift the boundary vertically according to $\Delta_{\sigma} \approx F^{-1/2}$. The boundary between regions 1 and 2 is for telescope/instrument temperature of 15°C . Other parameters: $\text{NEP} = 2 \times 10^{-16} \text{W Hz}^{-1/2}$, $\text{QE} = 0.80$.

Figure 2 is a low-dispersion plot of a high-resolution solar spectrum. This type of data is readily obtained for the Sun in any spectral region, or for bright stars from 1 to 5 μm . The relative flux calibration was obtained from a laboratory lamp, but it could equally well have been determined from a standard star. This capability of producing a very-high-resolution spectrum with broadband photometric integrity is a new and valuable tool for astronomers. The continuum can be determined by interpolation (perhaps with the aid of a synthetic model spectrum) from distant frequencies.

Such spectra have been used in a variety of abundance analyses for the Sun and stars. Results of abundance studies by FTS methods have been reviewed recently (66, 74). Examples include studies of C, N, O and isotopic abundances and of the H/H₂ ratio (48, 106) in cool stars. Among the few solar abundance studies was the determination of the solar nickel isotope ratio in a combined laboratory-solar investigation (10).

The Sun has been used to empirically calibrate the strengths of certain molecular transitions that are important in stellar spectroscopy. Recent examples include OH (36), C₂ (12), and CN (86). FTS laboratory spectroscopy continues to provide line positions and strengths for such molecules as OH (65), H₂O (29), and many, many others (for examples, see recent issues of the *Journal of Molecular Spectroscopy*). At present, most atomic lines in infrared stellar spectra are still unidentified (e.g. 75), but FTS laboratory measurements are producing large numbers of new identifications and are also radically improving our knowledge of line positions and atomic energy levels.

Sophisticated model atmospheres are indispensable for interpretation of solar and stellar spectra. Equally important are diagnostics for the choice

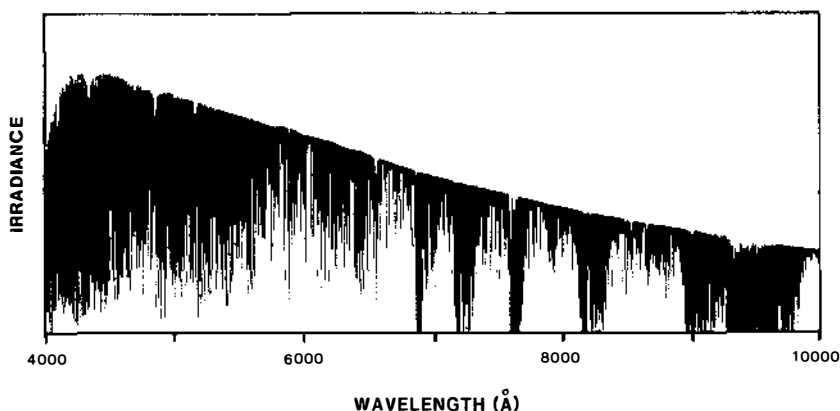


Figure 2 A compressed, high-resolution plot of the spectrum of the Sun in integrated light. Parameters: $\delta\sigma = 0.04 \text{ cm}^{-1}$, $t = 1 \text{ h}$, $\text{tel} = 1.5 \text{ m}$.

and verification of the models. Use of resonance-line profiles in the blue is complemented by measurement of the strong CO bands in the infrared. Heasley et al. (46) studied the 5- μm CO fundamental in Arcturus, and Tsuji (105) and Ayres & Testerman (3) observed these bands in the Sun. All three groups inferred the need for multicomponent models in the upper solar and stellar atmospheres.

Our empirical knowledge of solar and stellar convection, stellar rotation, and magnetic fields comes almost exclusively from line profiles. The FTS is well suited to record fully resolved profiles of low noise and high wavelength precision for the Sun and brighter stars. The subtle asymmetries in a line profile are often indiscernible in a normal spectral plot, even at high dispersion. A common method for emphasizing the deviations from symmetry is the bisector technique. The bisectors of chords across the profile at various depths may be plotted at greatly enhanced dispersion, as in Figure 3. These bisector curves by Livingston (61) show the characteristic C-shape observed in the Sun. The upward convecting regions of the photosphere, which contribute somewhat more than half of the emergent intensity, produce a blueshift in the central regions of the line profiles, while the stationary layer above the convection zone and the slowly convecting deep layers yield core and wing frequencies near the center-of-mass velocity (20). The velocity noise in a one-day sequence of such full-disk spectra is only 5 m s^{-1} .

A study of cool giants (72) found much more extreme effects, and an S-shaped bisector, suggestive of mass loss above the convective region. Hinkle et al. (47) have reported the time evolution of complex, multicomponent line profiles in Mira variables. They are able to distinguish numerous atmospheric regimes, including a rising pulsation wave, falling material, stationary overlying material, and several shells of ejected gas.

The IR spectrum is favorable for magnetic field studies, as the ratio of Zeeman splitting to Doppler width increases with wavelength. The unexpected discovery of atomic emission lines near $12 \mu\text{m}$ in the infrared solar spectrum (13, 68) provides an excellent example of line profiles useful as a probe of magnetic fields. The strongest of these lines have recently been shown by Chang & Noyes (15) to be due to high angular momentum states in neutral Mg and Al, with a Landé g -value of 1. Even with this relatively low value of g , they have the highest Zeeman sensitivity of any known lines. Figure 4 shows the Zeeman-split profiles for a number of magnetic regions on the solar surface. The emission is presumed to be chromospheric within a broader photospheric line; thus information about the field variation with depth is encoded in the profiles. In a stellar observation, Giampapa et al. (35) have measured the splitting of an Fe I line at 6388.65 cm^{-1} in the RS CVn star λ And; they detected a large field (1300 G).

In a unique series of observations, Stenflo et al. (87) have modified an FTS to function as a spectropolarimeter, and they have used this to survey the solar limb spectrum from 4200 to 9950 Å at high resolution. They report polarization effects in many lines, and discuss the results with reference to resonant and fluorescent scattering and quantum mechanical interference effects.

Low-resolution IR spectroscopy offers considerable scope for the FTS in stellar studies, but this area is not well developed (66, 74).

3.2 Planetary Astronomy

In 1969, Connes et al. (16) published their remarkable infrared atlas of the spectra of Venus, Mars, and Jupiter, and in so doing demonstrated the

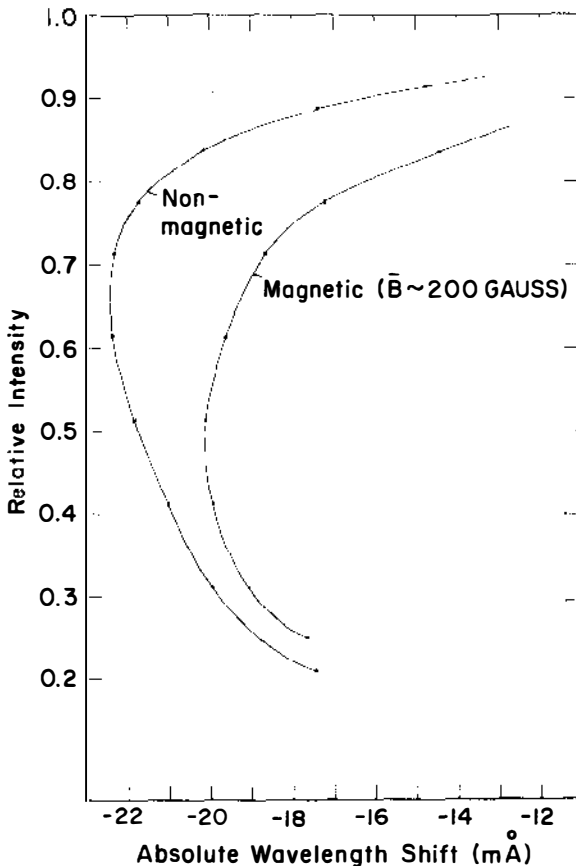


Figure 3 Typical FTS line bisectors for magnetic and nonmagnetic regions (61). The line is Fe 5250.6 Å. Parameters: aperture = 1' × 2', $\delta\lambda = 0.008 \text{ \AA}$, $t = 6 \text{ min}$.

information-gathering capability of an FTS. The further opening of the infrared in subsequent years has produced many pioneering investigations and contributed much to the revival of planetary spectroscopy.

Results obtained by Fourier transform spectroscopy include a large increase in the number of known chemical constituents of the solar system. Measured elemental abundances in the outer planets may determine the "cosmic" values, or they may instead reveal something about the planetary formation process; it is not yet clear which will be the case (33). The best estimate of the deuterium abundance should eventually come from the outer planets, although not without some effort (21, 23, 26, 53). Other work on planetary atmospheres has revealed stratospheric emission due to airglow on Mars and photochemistry on Jupiter, Saturn, and Titan (52, 64). Infrared spectra led to the discovery of the temperature inversion in the atmospheres of the giant planets, and they have since been employed to map the thermal structures of these atmospheres (70). Abundances of PH_3 and H_2O reveal the presence of nonequilibrium chemistry deep in the atmospheres of Jupiter and Saturn (53, 59). FTS spectra of Saturn have been used to study NH_3 in both gaseous and solid form (28) in an attempt to understand its low abundance there. Remote mineralogical analysis of solid planetary, ring, satellite, and asteroid materials is a rich field, with detections of various ices in the outer solar system and of a number of

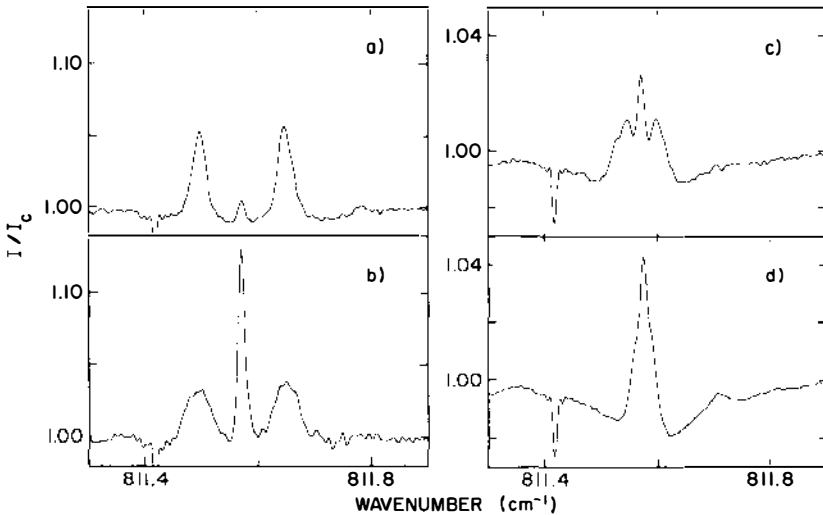


Figure 4 The solar emission line $7i \rightarrow 6h$ of Mg I at 811.575 cm^{-1} : (a) on the side of a large sunspot penumbra toward disk center; (b) on the side of the penumbra toward the limb; (c) and (d) in two locations in a plage near disk center (13). Parameters: $\delta\sigma = 0.005 \text{ cm}^{-1}$, $S/N \sim 10^3$, aperture $\leq 60 \text{ arcsec}^2$, $t = 10\text{--}60 \text{ min}$, tel = 1.5 m.

mineralogical groups that correlate with known meteoritic materials (24, 25, 30, 31, 57, 60). The only available IR spectrum of a comet was also obtained with an FTS (49).

Excellent recent reviews of planetary spectroscopy, with emphasis on FTS techniques, have been given by Fink & Larson (27), Larson (58), and Encrenaz & Combes (22). The results of the last few years are too numerous to list, but they are mostly concerned with the composition of the atmospheres of the outer planets. Lutz et al. (63) recorded a spectrum of Titan in the infrared H band. A portion of this spectrum (shown in Figure 5) shows the evidence for the detection of CO. This molecule was first sought as a possible vestigial remnant of the primordial solar nebula, although contemporary production by photochemical processes appears possible. In the course of a related laboratory study of methane, also employing Fourier spectroscopy, Lutz et al. (62) discovered a previously unknown band of CH_3D near 6427 cm^{-1} . It is present in their Titan spectrum and should yield an improved estimate of the D/H ratio.

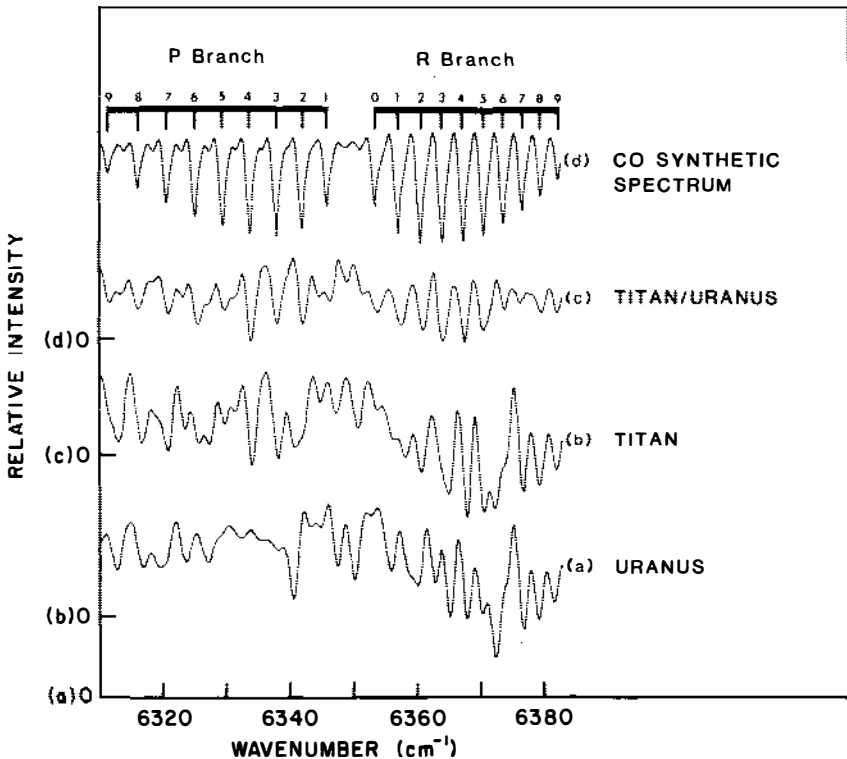


Figure 5 The detection of CO in the atmosphere of Titan (63). Parameters: $\delta\sigma = 1.2\text{ cm}^{-1}$, H filter, $m_H \sim 8.4$, $t = 7.5\text{ h}$, $\text{tel} = 4\text{ m}$.

Each Voyager spacecraft carried a Fourier spectrometer and obtained superb spectra of Jupiter, Saturn, and their satellites, with good spatial resolution and low noise, though only modest spectral resolution [Hanel et al. (41, 42, 44, 45)]. The spectrum of the North Equatorial Belt of Jupiter is shown in Figure 6 [Kunde et al. (53)]. This spectrum covers a wide spectral range with high photometric accuracy. It has been used to study the thermal balance of the atmosphere (70), the He/H ratio, and the possible existence of trace constituents. Ground-based spectroscopy, limited to atmospheric windows, can produce complementary information. In a coordinated observation from the ground, Tokunaga et al. (102) observed three regions on Jupiter with higher spectral resolution in a small bandpass. Their spectrum of the North Tropical Zone is shown in Figure 7. Although noisier, this spectrum reveals details of the molecular band structure and shows trace gases such as $^{15}\text{NH}_3$ and C_2H_6 .

Continuing activity shows that much remains to be done in planetary spectroscopy, and substantial improvements in sensitivity are badly needed. Many detected molecular bands have not yet been analyzed, and there is a persistent need for supporting laboratory spectroscopy. Since wide spectral coverage, high resolution, and accurate line profiles are important in this work, it is likely that Fourier spectroscopy will continue to serve this field.

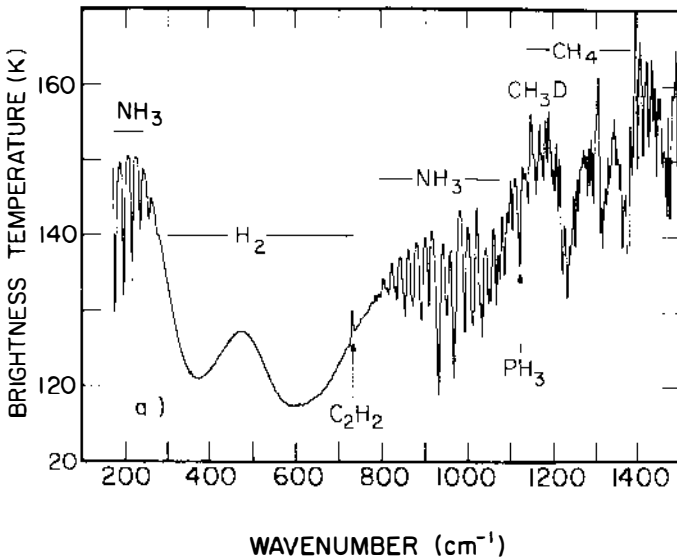


Figure 6 The mean spectrum of Jupiter's North Equatorial Belt, from *Voyager 1* (53). Parameters: $\delta\sigma = 4.3 \text{ cm}^{-1}$.

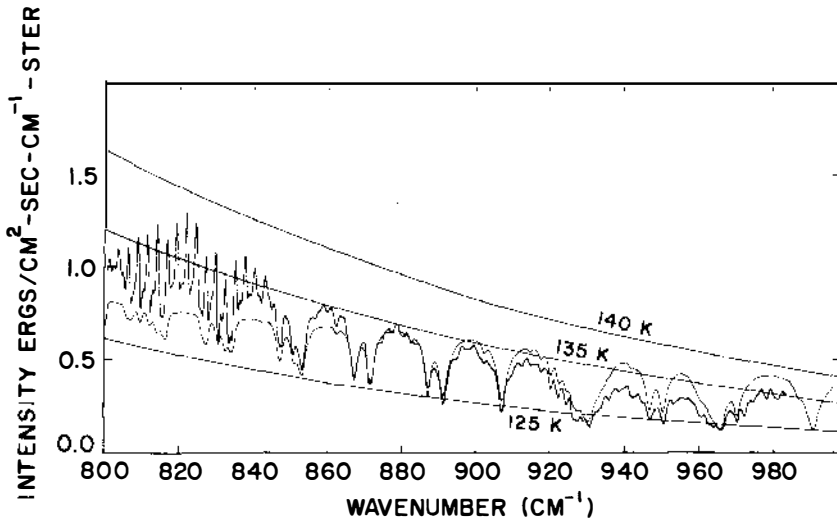


Figure 7 The ground-based mean spectrum of Jupiter's North Tropical Zone (dark curve), compared with a synthetic spectrum (light curve) (102). Parameters: $\delta\sigma = 1.1 \text{ cm}^{-1}$, aperture = $3.5''$, $t = 3 \text{ h}$, $\text{tel} = 4 \text{ m}$.

3.3 Young Stars, Molecular Clouds, and Gaseous Nebulae

The high extinction of molecular clouds precludes most visible observations. However, both the infrared and the radio regimes have been fruitfully employed to penetrate the obscuring dust. FTS spectroscopy has been particularly successful in revealing new phenomena associated with regions of star formation, especially including hydrogen $B\gamma$ emission from compact H II regions and stellar winds, and H_2 emission from shock fronts.

The Steward Observatory FTS (88) has been used in a survey program to reveal the major emission features from obscured sources in the $4000\text{--}6500 \text{ cm}^{-1}$ region (54, 90–93, 99, 101). An example is shown in Figure 8. The resolution is $\sim 130 \text{ km s}^{-1}$, which maximizes the sensitivity to lines of this width. Evaluation of the extinction by Thompson (94, 95) revealed excess line emission relative to the spectral type estimated from the total luminosity. These results have stimulated lively discussion of the deviations from recombination theory in a stellar wind or an ultradense H II region optically thick in the hydrogen lines, and of possible accretion disks (51, 84, 95, 96). In evaluating the line-formation process, line profiles are again of great importance. Hall et al. (37), Simon et al. (83, 84), and Scoville et al. (81) have examined profiles of $B\alpha$ and $B\gamma$ for several of these sources and found wide wings $> 100 \text{ km s}^{-1}$, suggestive of a stellar wind.

Only one obscured young star has been the subject of extensive study.

This is the BN source in the Orion molecular cloud OMC-1. Note that this cloud is behind the famous Orion H II nebula. A series of high-resolution FTS spectra has been obtained in the accessible portions of the 2–5 μm region (37, 78, 79, 81). These spectra reveal complex absorption and emission profiles in the CO transitions.

Figure 9, from Scoville et al. (81), shows the CO overtone vibration-rotation band. The emission from excited vibrational states indicates the remarkable excitation temperature $T_{\text{vib}} > 19,000$ K. This suggests that the molecular material is a useful probe to a region quite close to the exciting star. The absorption in Figure 9 shows a low excitation temperature, appropriate for the foreground molecular cloud.

Figure 10 [Scoville et al. (81)] shows a selection of line profiles from the CO vibration-rotation fundamental band near 5 μm . Two prominent absorption features are associated with the undisturbed foreground molecular cloud and with the expanding shell that is pushed out by some unknown energetic activity within the cloud. A strong emission feature,

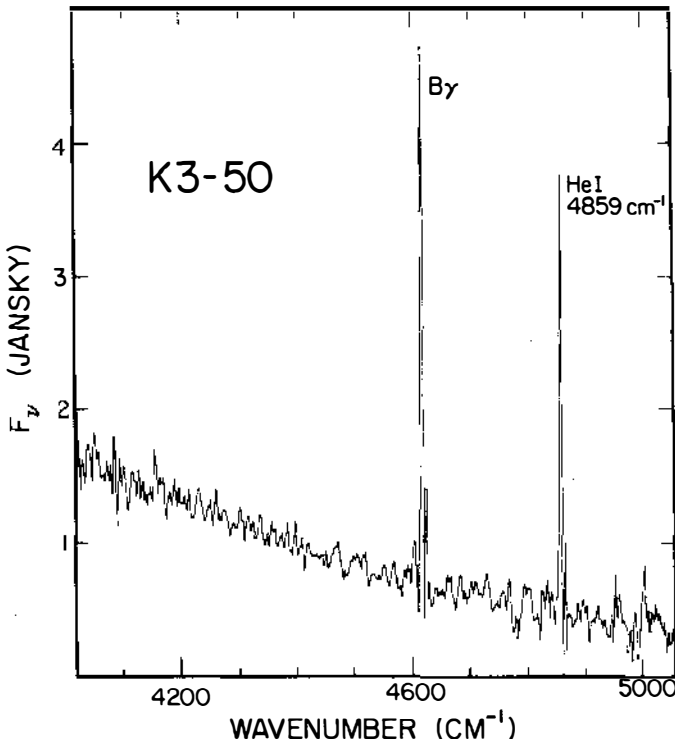


Figure 8 The obscured IR object K3-50 [Thompson & Tokunaga (93)]. Variation in continuum indicates typical noise. Parameters: $\delta\sigma = 2.0 \text{ cm}^{-1}$, K band, $t = 1$ h, $\text{tel} = 2.3$ m.

with low excitation temperature, is quite distinct from the hot emission seen in Figure 9. Yet another possible absorption feature has the dynamical signature appropriate to infalling material. The disentanglement of this spectral detail appears to require multiple sources or a nonspherical geometry. Possibilities include a remnant disk and a bow shock (81). A particular puzzle from the high-resolution data is that the sources studied thus far (BN, CRL 490, and M17 IRS1) all have substantial velocities relative to their surrounding molecular cloud, suggestive of rapid escape from the presumed place of birth.

The discovery of molecular hydrogen emission from the Orion molecular cloud (32) provided a new and unexpected probe of the cloud interior. It is generally believed that these emission lines are a cooling mechanism for shock-heated material, although this picture does not provide a fully satisfactory understanding of the phenomenon. Active observational work by the FTS, the Fabry-Perot, and other means has extended the known sites of H_2 emission to include T Tauri stars, Herbig-Haro objects, planetary nebulae, and supernova remnants (6). An airborne observation by Davis et al. (19) is shown in Figure 11. The resolution is $\sim 90 \text{ km s}^{-1}$, similar to the known line widths. The advantage of working at high altitude lies in the possibility of observing lines that are partially or totally obscured from the ground, as is the case for some of the O - and Q -branch lines. In this

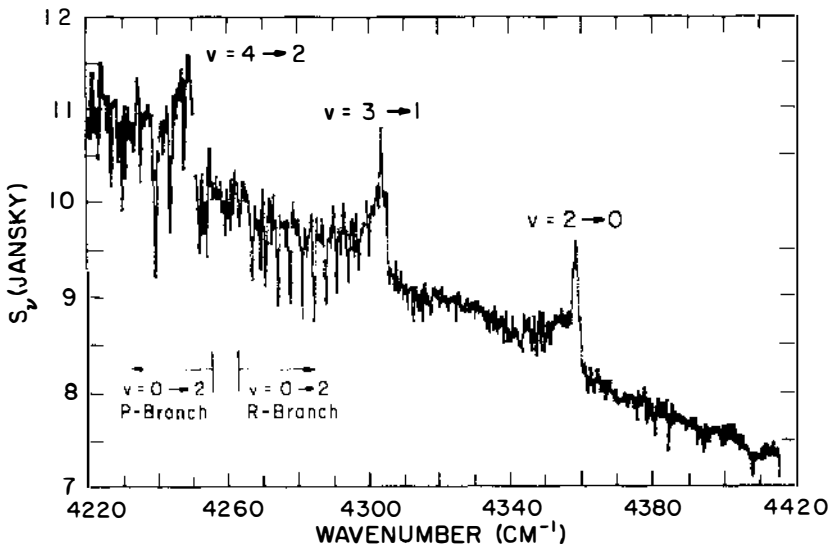


Figure 9 CO $v = 2 \rightarrow 0$ absorption and emission from the BN source (81). Parameters: $\delta\sigma = 0.3 \text{ cm}^{-1}$, K band, $m_K \sim 5.0$, $t = 4.8 \text{ h}$, $\text{tel} = 4 \text{ m}$.

spectrum the H_2 emission is from deep within the cloud, while the H I emission is from the foreground H II region.

Considerable attention has been given to the question of the extinction in front of the H_2 emission regions. This is critical in estimating the energetics and the geometry. High-resolution measurements of the S - and Q -branch lines have been obtained in order to estimate reddening. A selection of resolved profiles is shown in Figure 12 from Scoville et al. (80). The authors consider the possibility that the blue and red wings arise in different regions of the cloud and have different extinction. They find that the most highly blueshifted emission is more reddened than the low-velocity emission.

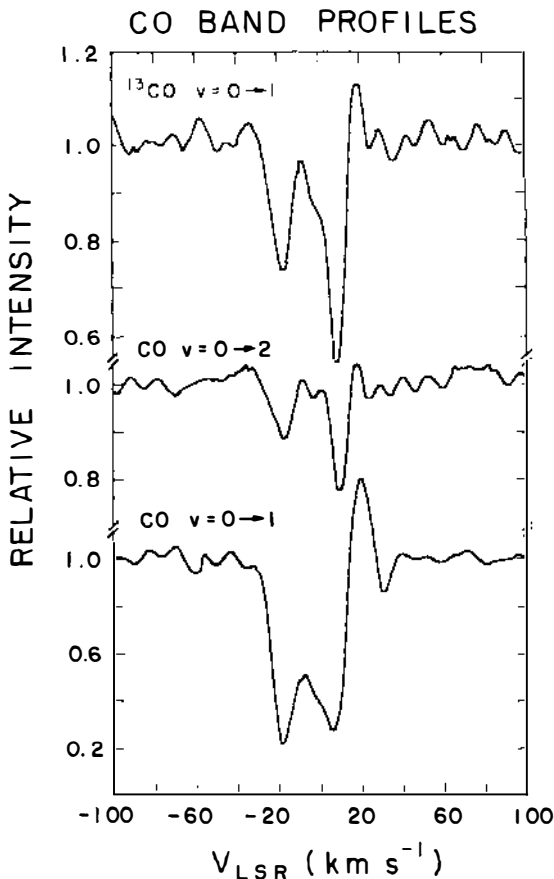


Figure 10 CO $v = 1 \rightarrow 0$ and $2 \rightarrow 0$ line profiles in the BN spectrum (81). Parameters: $\text{res} = 7 \text{ km s}^{-1}$, $m_K \sim 5.0$, $m_L \sim 1.7$, $\text{tel} = 4 \text{ m}$.

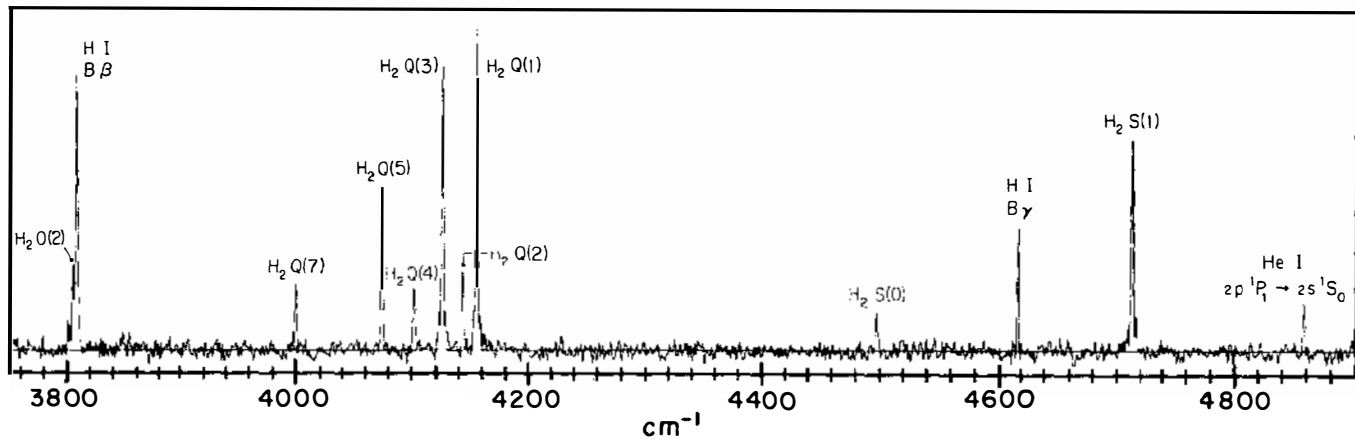


Figure 11 Airborne spectrum of the Orion H₂ source (19). Parameters: $\delta\sigma = 1.2 \text{ cm}^{-1}$, $2.1\text{--}2.7 \mu\text{m}$, $t = 150 \text{ min}$, $\text{tel} = 0.9 \text{ m}$.

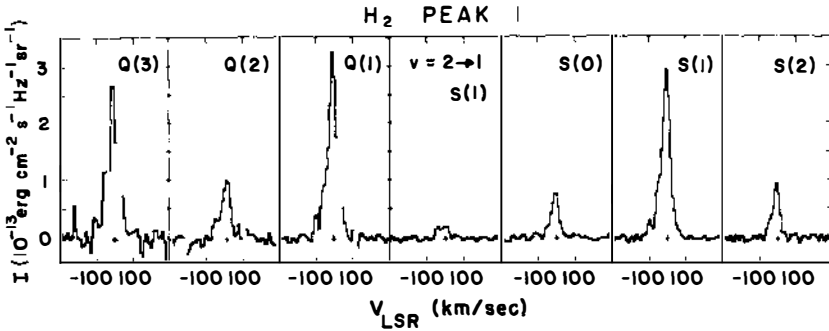


Figure 12 High-resolution spectrum of the H_2 band in emission peak 1 in Orion (80). Parameters: $\delta\sigma = 0.3 \text{ cm}^{-1}$, K band, aperture = $3.75''$, $t = 70 \text{ min}$, tel = 4 m.

FTS studies in the IR have also been extended to galactic nebulae. These studies have included detection and study of H_2 emission (85, 104), measurement of H I and He I emission-line widths (100), and unsuccessful attempts to resolve line structure in the mysterious $3.3\text{-}\mu\text{m}$ emission feature (103). Airborne, high-resolution spectra in the far-IR have been obtained to study the abundances and cooling processes in H II regions [for example, in M8, M17, and NGC 7538 (5, 67)].

Substantial observational effort in the radio and IR is aimed at identifying protoplanetary nebulae. FTS studies near $2 \mu\text{m}$ have produced evidence that one candidate, HM Sag, almost certainly is not one, as it shows evidence of a cool-star spectrum (98). CRL 618, however, which has both H I and H_2 emission from a complicated structure, might be (97).

3.4 Mass Loss from Evolved Stars

The study of mass loss is an ideal area for the application of the FTS technique. Line profiles at the highest resolution are required, and many transitions are needed to explore a range of excitation temperatures. This subject is still in a primitive state of development because of the difficulties of coupling observation and theory. On the theoretical side, it is not clear how mass loss occurs. In cool, luminous stars, mass loss is observed to be accompanied by a dusty circumstellar envelope. Grains can be expelled by radiation pressure under some conditions, but static stellar models do not produce grains in sufficient abundance to account for observed mass loss rates. Interpretation of the observational material is at an impasse because of the inability to assign a radius to the inner boundary of the circumstellar shell. Infrared studies hold the promise of deducing the spatial extent of the shell from the excitation temperature of the spectrum. Particularly attractive is the availability of many tens of transitions of the CO molecule from the ground vibrational state. Owing to its high dissociation energy,

CO is expected to be stable from the photosphere of the cool star out through the shell.

The most extensive case studies of cool-star mass loss based on IR FTS data are for χ Cyg (47), α Ori (7), and IRC + 10216 (50, 73). Figure 13 shows a line profile extracted from a spectrum of the CO fundamental band in the M supergiant α Ori. This profile reveals several components. The telluric CO line, which has not been removed in the reduction, shows the position of the unshifted line. The very broad stellar photospheric line reaches a depth of only about 70%, typical of strong photospheric lines in this spectral region. Narrow circumstellar absorption appears with two distinct components, S1 and S2, which clearly differ in Doppler shift. From inspection of many lines of differing lower-state excitation, it is possible to estimate the rotational temperature of the CO. The S1 component has $T_{\text{rot}} \sim 200$ K, and S2 has $T_{\text{rot}} \sim 70$ K. This reveals a common feature of late-type stellar shells: The material is apparently clumped in discrete velocity regimes, with the rotational temperature decreasing with increasing expansion velocity (8, 71).

A long observational study of χ Cyg, an S-type long-period variable, has provided a possible clue to the cool-star mass loss process by discovering a warm, stationary shell of gas above the pulsating photosphere [Hinkle et al. (47)]. The authors speculate that dynamic activity may support a grain-forming region at several stellar radii, from which outward acceleration may begin. The detection of discrete shells suggests that either the outflow is modulated and episodic, or that the acceleration is accomplished in some sense impulsively, rather than continuously (71).

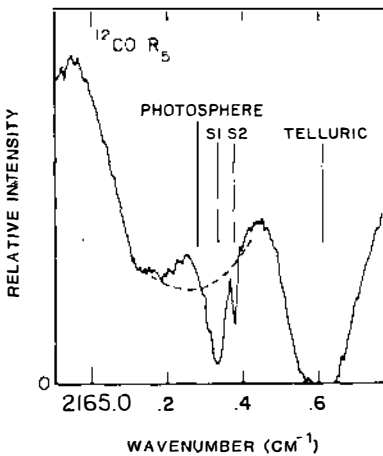


Figure 13 CO vibration-rotation 1 \rightarrow 0 R(5) line in α Ori. [Bernat et al. (7)]. Parameters: $\delta\alpha = 0.006$ cm⁻¹, 2110–2200 cm⁻¹, S/N = 95, $t = 180$ min, tel = 4 m.

An extensive series of observations of IRC + 10216, as well as a detailed interpretation by numerical modeling, has been used to estimate parameters of mass loss in this extreme case (50). Figure 14 shows an interesting comparison between line profiles of CO rotational transitions, measured in the millimeter radio spectrum (69), and profiles of CO vibration-rotation transitions from the infrared. The millimeter profiles are of purely emission lines, taken with an antenna that did not resolve the source structure (typical in such measurements). Emission is detected equally from the front and back sides of the shell. The two CO species show profiles characteristic of optically thick and optically thin emission in an expanding spherical shell. The IR profiles show velocity structure in the foreground shell, and P Cygni emission from near the source.

The infrared profiles contain much more, though different, information. First, the absorption component is formed against the continuum source, and thus the profiles are not blurred seriously by projection effects. Consequently, it is possible to distinguish considerable structure in the shell dynamics, as discussed above. In this case, IRC + 10216 has 3 distinct shells, with $T_{\text{rot}} \sim 700, 300, \text{ and } 120 \text{ K}$, respectively, and with increasing expansion velocity. Second, the emission component of the 1-0 lines is formed close to the star, and it shows the effects of obscuration of the back side of the

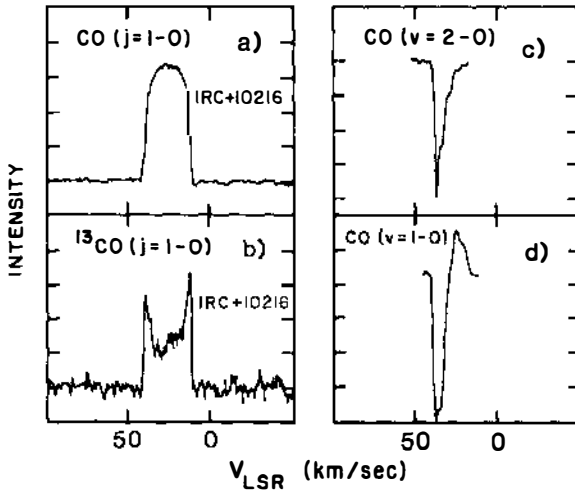


Figure 14 CO emission and absorption in the IRC + 10216 circumstellar shell [Keady (50)]. Millimeter emission from (a) the optically thick $^{12}\text{CO } J = 1 \rightarrow 0$ line and (b) the optically thin $^{13}\text{CO } J = 1 \rightarrow 0$ line. Infrared absorption-emission profiles from (c) the $v = 2 \rightarrow 0$ band and (d) the $v = 1 \rightarrow 0$ band.

emission shell. Finally, a broad, shallow absorption, attributed to the photospheric line, may show effects of scattering from the expanding dust shell. In sum, the IR line shows one emission and four absorption components, whereas the millimeter spectrum showed one in emission. However, for measuring the total shell mass, or for detecting minor constituents, the millimeter measurement is far more sensitive to the large volume of material at large radius from the source. Keady (50) estimates a mass loss of $10^{-4} M_{\odot} \text{ yr}^{-1}$, and he finds that several regimes of acceleration can account for the peculiar velocity structure of the lines.

A number of F supergiants have been determined to have high mass loss rates. It seems unlikely that dust plays a role in the ejection process. The infrared region, especially the CO molecule, is nevertheless a good diagnostic for the shells of these stars. Thompson & Boroson (89) studied infrared Na I and Mg I emission in the wind or shell of IRC + 10420. They attributed the emission to UV pumping of the upper levels and inferred a high density of material above the photosphere. Lambert et al. (55) used IR spectra of CO to investigate the photospheric and circumstellar mass motions around ρ Cas and HR 8752. In 1975 the latter star apparently ejected a discrete shell, which has decelerated and is now falling back. Pulsations in the underlying photosphere have also been monitored.

3.5 *Galactic Nuclei*

The nuclear regions of our own and other galaxies are within reach of an FTS, although at very modest spectral resolution. The center of our Galaxy is sufficiently close that we may distinguish several discrete components, both extended and pointlike. In spite of an estimated 30 magnitudes of visual extinction to the galactic center, infrared spectroscopy of these sources is possible. Several of the point sources are found to be late-type supergiants or star clusters (2, 40, 107). Doppler shifts of these may be used to probe the virial mass of the galactic center and eventually, perhaps, some of the stellar parameters.

In Figure 15, from Hall et al. (40), the spectrum of IRS 7 shows the CO bands characteristic of a cool, high-luminosity star. Figure 15 also displays the spectrum of IRS 16, the slightly extended source at the center of the far-infrared emission region. Weak stellar CO indicates a contribution from a spectral type earlier than K0, or perhaps spectral dilution by continuum emission from a nonstellar source. Emission from ionized gas, also evident in the spectrum of IRS 16, provides another indication of activity in the galactic core. The interest in the gaseous emission hinges on the line profiles. Wollman et al. (107) found a complex $B\gamma$ profile, with narrow and broad components, while Hall et al. (40) determined a remarkable velocity width of 2000 km s^{-1} for the He II line at $2.06 \mu\text{m}$. These flows are probably

determined by an unknown combination of gravitational, radiative, and other forces, and the interpretation may not be straightforward.

A spectrum of the central region of the spiral galaxy M81 was obtained by Aaronson (1). The CO bands at 4300 cm^{-1} were detected, confirming the assumption of earlier filter photometry that a depression there is due to CO in cool stellar photospheres. A number of active galactic nuclei have been studied. Rieke et al. (76) measured CO absorption and $B\gamma$ emission in spectra of the IR luminous galaxies M82 and NGC 253. They found that star-burst models with a dearth of low-mass stars could account for many of the observed characteristics of these nuclei.

Infrared spectra of the central regions of the bright Seyfert galaxies NGC 4151 and NGC 1068 have been recorded. Rieke & Lebofsky (77) combined a variety of spectrally and spatially resolved data to interpret the continuum and line emission detected from NGC 4151. They gave particular emphasis to the role of dust, which evidently is present in both the broad and narrow emission-line regions of the nucleus. An interesting comparison is found in the NGC 1068 observations of Hall et al. (39). Their

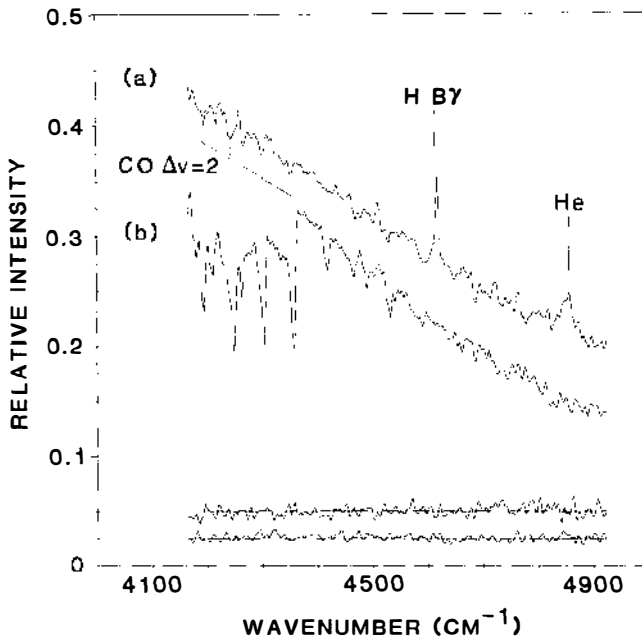


Figure 15 Galactic center sources: (a) IRS 16; (b) IRS 7 (40). Parameters: $\delta\sigma = 3.0\text{ cm}^{-1}$, K band, $m_K \sim 6.7, 8.4$, $t = 70, 170\text{ min}$, $\text{tel} = 4\text{ m}$.

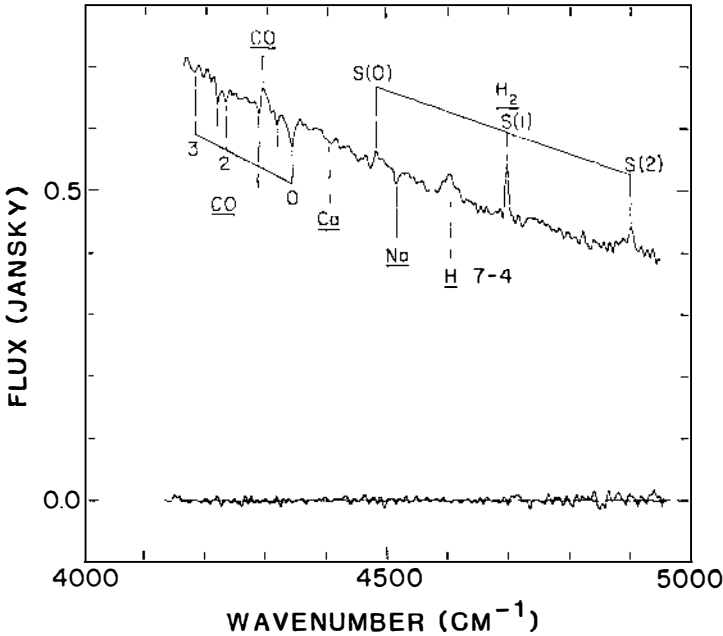


Figure 16 NGC 1068 (39). Parameters: $\delta\sigma = 5.0 \text{ cm}^{-1}$, K band, $m_K \sim 7.8$, $t = 8 \text{ h}$, $\text{tel} = 4 \text{ m}$.

spectrum appears in Figure 16. It shows cool-star absorption, broad $\text{Br}\gamma$ emission, narrow H_2 emission, hot dust, and possibly CO emission. The authors discussed analogies with sites of star formation in galactic molecular clouds and suggested that similar activity takes place on a very large scale in NGC 1068.

4. CONCLUSION

FTS methods have contributed in depth to a broad range of astrophysical research in the laboratory, the solar system, the Galaxy, and beyond. The FTS has surely more than fulfilled the dreams of the pioneers who brought it to fruition; it is now a unique and well-established tool for the observation of astronomical sources.

ACKNOWLEDGMENTS

We are grateful to Richard Joyce, John Keady, Harold Larson, John Leibacher, Michael Merrill, and Roger Thompson for reading and commenting on a draft of this paper.

Literature Cited

1. Aaronson, M. 1981. See Ref. 108, pp. 297–316
2. Augason, G. C., Smith, H. A., Wollman, E. R., Larson, H. P., Johnson, H. R. 1982. In *The Galactic Center*, ed. G. R. Riegler, R. D. Blandford, pp. 82–84. New York: Am. Inst. Phys. 216 pp.
3. Ayres, T. R., Testerman, L. 1981. *Ap. J.* 245: 1124–40
4. Baluteau, J. P., Anderegg, M., Moorwood, A. F. M., Coron, N., Beckman, J. E., et al. 1977. *Appl. Opt.* 16: 1834–40
5. Baluteau, J. P., Moorwood, A. F. M., Biraud, Y., Coron, N., Anderegg, M., Fitton, B. 1981. *Ap. J.* 244: 66–75
6. Beckwith, S. 1981. See Ref. 108, pp. 167–78
7. Bernat, A. P., Hall, D. N. B., Hinkle, K. H., Ridgway, S. T. 1979. *Ap. J. Lett.* 233: L135–39
8. Bernat, A. P. 1981. *Ap. J.* 246: 184–92
9. Brault, J. W. 1979. *Ossni. Mem. Oss. Astrofis. Arcetri* 106: 33–50
10. Brault, J. W., Holweger, H. 1981. *Ap. J. Lett.* 249: L43–46
11. Brault, J. W. 1982. *Philos. Trans. R. Soc. London Ser. A* 307: 503–11
12. Brault, J. W., Delbouille, L., Grevesse, N., Roland, G., Sauval, A. J., Testerman, L. 1982. *Astron. Astrophys.* 108: 201–5
13. Brault, J. W., Noyes, R. W. 1983. *Ap. J. Lett.* 269: L61–66
14. Carrington, A., Ramsay, D. A., eds. 1982. *Molecules in Interstellar Space*. London: R. Soc. 167 pp.
15. Chang, E. C., Noyes, R. W. 1983. *Ap. J. Lett.* 275: L11–13
16. Connes, J., Connes, P., Maillard, J.-P. 1969. *Atlas of Near Infrared Spectra of Venus, Mars, Jupiter and Saturn*. Paris: CNRS. 475 pp.
17. Connes, P. 1970. *Ann. Rev. Astron. Astrophys.* 8: 209–30
18. Davis, D. S., Larson, H. P., Williams, M., Michel, G., Connes, P. 1980. *Appl. Opt.* 19: 4138–55
19. Davis, D. S., Larson, H. P., Smith, H. A. 1982. *Ap. J.* 259: 166–79
20. Dravins, D., Lindegren, L., Nordlund, Å. 1981. *Astron. Astrophys.* 96: 345–64
21. Drossart, P., Encrenaz, T., Kunde, V., Hanel, R., Combes, M. 1982. *Icarus* 49: 416–26
22. Encrenaz, T., Combes, M. 1981. See Ref. 108, pp. 1–34
23. Encrenaz, T., Combes, M. 1982. *Icarus* 52: 54–61
24. Feierberg, M. A., Lebofsky, L. A., Larson, H. P. 1981. *Geochim. Cosmochim. Acta* 45: 971–81
25. Feierberg, M. A., Larson, H. P., Chapman, C. R. 1982. *Ap. J.* 257: 361–72
26. Fink, U., Larson, H. P. 1978. *Science* 201: 343–45
27. Fink, U., Larson, H. P. 1979. In *Fourier Transform Infrared Spectroscopy: Applications to Chemical Systems*, eds. J. R. Ferraro, L. J. Basile, 2: 243–315. New York: Academic. 336 pp.
28. Fink, U., Larson, H. P., Bjoraker, G. L., Johnson, J. R. 1983. *Ap. J.* 268: 880–88
29. Flaud, J.-M., Camy-Peyret, C., Maillard, J.-P., Guelachvili, G. 1977. *J. Mol. Spectrosc.* 65: 219–28
30. Fraundorf, P., Patel, R. I., Freeman, J. J. 1981. *Icarus* 47: 368–80
31. Gaffey, M. J., McCord, T. B. 1979. See Ref. 34, pp. 688–723
32. Gautier, T. N., Fink, U., Treffers, R., Larson, H. P. 1976. *Ap. J. Lett.* 207: L129–33
33. Gautier, D., Bezard, B., Marten, A., Baluteau, J. P., Scott, N., et al. 1982. *Ap. J.* 257: 901–12
34. Gehrels, T., ed. 1979. *Asteroids*. Tucson: Univ. Ariz. Press. 1181 pp.
35. Giampapa, M. S., Golub, L., Worden, S. P. 1983. *Ap. J. Lett.* 268: L121–25
36. Goldman, A., Murcray, F. J., Gillis, J. R., Murcray, D. G. 1981. *Ap. J. Lett.* 248: L133–35
37. Hall, D. N. B., Kleinmann, S. G., Ridgway, S. T., Gillett, F. C. 1978. *Ap. J. Lett.* 223: L47–50
38. Hall, D. N. B., Ridgway, S. T., Bell, E. A., Yarborough, J. M. 1979. *Proc. Soc. Photo-Optical Instrum. Eng.* 172: 121–29
39. Hall, D. N. B., Kleinmann, S. G., Scoville, N. Z., Ridgway, S. T. 1981. *Ap. J.* 248: 898–905
40. Hall, D. N. B., Kleinmann, S. G., Scoville, N. Z. 1982. *Ap. J. Lett.* 260: L53–57
41. Hanel, R., Conrath, B., Flasar, M., Herath, L., Kunde, V., et al. 1979. *Science* 206: 952–56
42. Hanel, R., Conrath, B., Flasar, M., Kunde, V., Lowman, P., et al. 1979. *Science* 204: 972–76
43. Hanel, R., Crosby, D., Herath, L., Vanous, D., Collins, D., et al. 1980. *Appl. Opt.* 19: 1391–1400
44. Hanel, R., Conrath, B., Flasar, F. M., Kunde, V., Maguire, W., et al. 1981. *Science* 212: 192–200
45. Hanel, R., Conrath, B., Flasar, F. M., Kunde, V., Maguire, W., et al. 1982. *Science* 215: 544–48

46. Heasley, J. N., Ridgway, S. T., Carbon, D. F., Milkey, R. W., Hall, D. N. B. 1978. *Ap. J.* 219: 970-78
47. Hinkle, K. H., Hall, D. N. B., Ridgway, S. T. 1982. *Ap. J.* 252: 697-714
48. Johnson, H. R., Goebel, J. H., Goorvitch, D., Ridgway, S. T. 1983. *Ap. J. Lett.* 270: L63-67
49. Johnson, J. R., Fink, U., Larson, H. P. 1983. *Ap. J.* 270: 769-77
50. Keady, J. J. 1982. *The circumstellar envelope of IRC+10216*. PhD thesis. N. Mex. State Univ., Las Cruces
51. Krolik, J. H., Smith, H. A. 1981. *Ap. J.* 249: 628-36
52. Kunde, V. G., Aikin, A. C., Hanel, R. A., Jennings, D. E., Maguire, W. C., Samuelson, R. E. 1981. *Nature* 292: 686-88
53. Kunde, V., Hanel, R., Maguire, W., Gautier, D., Baluteau, J. P., et al. 1982. *Ap. J.* 263: 443-67
54. Lada, C. J., Gautier, T. N. 1982. *Ap. J.* 261: 161-69
55. Lambert, D. L., Hinkle, K. H., Hall, D. N. B. 1981. *Ap. J.* 248: 638-50
56. Larson, H. P., Fink, U. 1975. *Appl. Opt.* 14: 2085-95
57. Larson, H. P., Veeder, G. J. 1979. See Ref. 34, pp. 724-44
58. Larson, H. P. 1980. *Ann. Rev. Astron. Astrophys.* 18: 43-75
59. Larson, H. P., Fink, U., Smith, H. A., Davis, D. S. 1980. *Ap. J.* 240: 327-37
60. Lebofsky, L. A., Feierberg, M. A., Tokunaga, A. T., Larson, H. P., Johnson, J. R. 1981. *Icarus* 48: 453-59
61. Livingston, W. C. 1982. *Nature* 297: 208-9
62. Lutz, B. L., de Bergh, C., Maillard, J.-P., Owen, T., Brault, J. 1981. *Ap. J. Lett.* 248: L141-45
63. Lutz, B. L., de Bergh, C., Owen, T. 1983. *Science* 220: 1374-75
64. Maguire, W. C., Hanel, R. A., Jennings, D. E., Kunde, V. G., Samuelson, R. E. 1981. *Nature* 292: 683-86
65. Maillard, J.-P., Chauville, J., Mantz, A. 1976. *J. Mol. Spectrosc.* 63: 120-41
66. Merrill, K. M., Ridgway, S. T. 1979. *Ann. Rev. Astron. Astrophys.* 17: 9-41
67. Moorwood, A. F. M., Baluteau, J.-P., Anderegg, M., Coron, N., Biraud, Y., Fitton, B. 1980. *Ap. J.* 238: 565-76
68. Murcray, F. J., Goldman, A., Murcray, F. H., Bradford, C. M., Murcray, D. G., et al. 1981. *Ap. J. Lett.* 247: L97-99
69. Olofsson, H., Johansson, L. E. B., Hjalmarsson, Å., Rieu, N.-G. 1982. *Astron. Astrophys.* 107: 128-44
70. Orton, G. S. 1981. See Ref. 108, pp. 35-56
71. Ridgway, S. T. 1981. In *Physical Processes in Red Giants*, ed. I. Iben, A. Renzini, pp. 305-9. Dordrecht: Reidel. 488 pp.
72. Ridgway, S. T., Friel, E. D. 1981. In *Effects of Mass Loss on Stellar Evolution*, ed. C. Chiosi, R. Stalio, pp. 119-24. Dordrecht: Reidel. 566 pp.
73. Ridgway, S. T., Keady, J. J. 1982. See Ref. 14, pp. 33-38
74. Ridgway, S. T. 1984. In *Galactic and Extragalactic Infrared Spectroscopy*, ed. M. F. Kessuer, J. P. Phillips, pp. 309-30. Dordrecht: Reidel
75. Ridgway, S. T., Carbon, D. F., Hall, D. N. B., Jewell, J. 1984. *Ap. J. Suppl.* 54: 177-210
76. Rieke, G. H., Lebofsky, M. J., Thompson, R. I., Low, F. J., Tokunaga, A. T. 1980. *Ap. J.* 238: 24-40
77. Rieke, G. H., Lebofsky, M. J. 1981. *Ap. J.* 250: 87-97
78. Scoville, N. Z. 1981. See Ref. 14, pp. 23-32
79. Scoville, N. Z. 1981. See Ref. 108, pp. 187-205
80. Scoville, N. Z., Hall, D. N. B., Kleinmann, S. G., Ridgway, S. T. 1982. *Ap. J.* 253: 136-48
81. Scoville, N. Z., Kleinmann, S. G., Hall, D. N. B., Ridgway, S. T. 1983. *Ap. J.* 275: 201-24
82. Deleted in proof
83. Simon, M., Righini-Cohen, G., Fischer, J., Cassar, L. 1981. *Ap. J.* 251: 552-56
84. Simon, M., Felli, M., Cassar, L., Fischer, J., Massi, M. 1983. *Ap. J.* 266: 623-45
85. Smith, H. A., Larson, H. P., Fink, U. 1981. *Ap. J.* 244: 835-43
86. Sneden, C., Lambert, D. L. 1982. *Ap. J.* 259: 381-91
87. Stenflo, J. O., Twerenbold, D., Harvey, J. W., Brault, J. 1983. *Astron. Astrophys. Suppl.* 54: 505-14
88. Thompson, R. I., Reed, M. A. 1975. *Publ. Astron. Soc. Pac.* 87: 929-32
89. Thompson, R. I., Boroson, T. A. 1977. *Ap. J. Lett.* 216: L75-77
90. Thompson, R. I., Tokunaga, A. T. 1978. *Ap. J.* 226: 119-23
91. Thompson, R. I., Tokunaga, A. T. 1979. *Ap. J.* 229: 153-57
92. Thompson, R. I., Tokunaga, A. T. 1979. *Ap. J.* 231: 736-41
93. Thompson, R. I., Tokunaga, A. T. 1980. *Ap. J.* 235: 889-93
94. Thompson, R. I. 1981. See Ref. 108, pp. 153-66
95. Thompson, R. I. 1982. *Ap. J.* 257: 171-78
96. Thompson, R. I., Thronson, H. A., Campbell, B. 1983. *Ap. J.* 266: 614-22
97. Thronson, H. A. 1981. *Ap. J.* 248: 984-91

98. Thronson, H. A., Harvey, P. M. 1981. *Ap. J.* 248: 584-90
99. Thronson, H. A., Thompson, R. I. 1982. *Ap. J.* 254: 543-49
100. Thronson, H. A. 1983. *Ap. J.* 264: 599-604
101. Tokunaga, A. T., Thompson, R. I. 1979. *Ap. J.* 229: 583-86
102. Tokunaga, A. T., Knacke, R. F., Ridgway, S. T. 1980. *Icarus* 44: 93-101
103. Tokunaga, A. T., Young, E. T. 1980. *Ap. J. Lett.* 237: L93-96
104. Treffers, R. R., Fink, U., Larson, H. P., Gautier, T. N. 1976. *Ap. J.* 209: 793-99
105. Tsuji, T. 1977. *Publ. Astron. Soc. Jpn.* 29: 497-510
106. Tsuji, T. 1983. *Astron. Astrophys.* 122: 314-21
107. Wollman, E. R., Smith, H. A., Larson, H. P. 1982. *Ap. J.* 258: 506-14
108. Wynn-Williams, C. G., Cruikshank, D. P., eds. 1981. *Infrared Astronomy*. Dordrecht: Reidel. 376 pp.